EUROPEAN JOURNAL OF PURE AND APPLIED MATHEMATICS
2025, Vol. 18, Issue 4, Article Number 6764
ISSN 1307-5543 – ejpam.com
Published by New York Business Global

Novel Quasi-Periodic Type Optical Solitons and the Formation of Fractal Structures in Non-integrable Nonlinear Helmholtz Equations with Phase Portraits and Chaotic Analysis

Khaled Suwais[1], Nabil Mlaiki[2], Shoaib Barak[3], Rashid Ali[4,*]

[1] *Faculty of Computer Studies, Arab Open University, Riyadh 11681, Saudi Arabia*
[2] *Department of Mathematics and Sciences, Prince Sultan University, Riyadh 11586, Saudi Arabia*
[3] *Department of Mathematics, Government Degree College Number 2, Mardan 23200, Pakistan*
[4] *School of Mathematical Sciences, Zhejiang Normal University, Jinhua 321004, P.R. China*

Abstract. In this study, we consider new optical soliton solutions of one of the most important non-integrable model arising in optical fibres, namely Nonlinear Helmholtz equations (NHEs) that describes transverse interactions, transmission of coupled waves and optical solitons' propagation in the field of fiber optics. We apply an adapted method to obtain some novel plethora of optical quasi-periodic soliton solutions. These solutions are presented in the shape of exponential, hyperbolic, trigonometric and rational functions. A set of 3D visualization, contour plots and 2D curves of these solutions physical relevance are presented with implications for the nonlinear optics. These figures also reveal that the established optical solitons exhibit quasi-periodicity due to the combination of linear periodic and axial perturbations, and that the presence of quasi-periodical perturbations of the solitons leads to the formation of the fractal-like structures. We also study the chaotic/periodic and bifurcation behavior, associated with the model, in the light of Hamiltonian analysis, as a consequence, we find positive results of the quasi-periodicity and fractal-like structures in the systems under consideration. Apart from offering novel analytical perspectives for dealing with the coupled NHEs, the present results would also be a concrete contribution to the understanding the soliton wave dynamics in complicated nonlinear media.

2020 Mathematics Subject Classifications: 35Q55, 37N20, 37G35

Key Words and Phrases: Nonlinear Helmholtz equations, unified method, complex structured partial differential equations, optical fractals, quasi-periodic soliton, phase portraits, chaotic analysis

*Corresponding author.
DOI: https://doi.org/10.29020/nybg.ejpam.v18i4.6764

Email addresses: khaled.suwais@arabou.edu.sa (K. Suwais), nmlaiki@psu.edu.sa, nmlaiki2012@gmail.com (N. Mlaiki), shoaibbarak2015@gmail.com (S. Barak), rashidali0887@gmail.com (R. Ali)

1. Introduction

Nonlinear Partial Differential Equations (NPDEs) are applied in many areas of science [1]-[5]. Notable among them are the Higgs model in particle physics, the Drinfeld-Sokolov-Wilson system found in fluid dynamics, the Duffing equation for periodic motions the nonlinear Maccari's system in hydrodynamics, the Gilson-Pickering equation in theory of crystal lattice and plasma physics, the Kairat equations in optics, coupled NHEs in optics etc. Several analytical and numerical techniques with exact and numerical solutions are introduced by the academicians to study the mechanism of NPDEs. However, the NPDEs are far from being easy, consider few obstacles spanning from single solution and the partner who gets none to the sensitivity to initial conditions, the lack of a precise definition of the exact solution and the complexity of nonlinearity. In the class of exact solutions the case of traveling wave solutions is of special interest, in particular, solitonic solutions provide useful information on the dynamical behavior of nonlinear models. In order to investigate the soliton theory of such non-linear models having the ability to provide information of underlying physical phenomena, a number of efficient methods to obtain soliton solutions have been developed in the last few years. These methods are based on Matlab, Maples, Mathematica and other symbolic computer systems that ease complicated algebraic calculations. These include extended direct algebraic method [6], tanh-coth approach [7], Poincar'e-Lighthill-Kuo technique [8], sine-cosine strategy [9], Jacobi elliptic function methodology [10], (G'/G)-expansion approach [11]-[13], Khater technique [14], Hirota bilinear approach [15], sub-equation strategy [16], Kudryashov technique [17], modified simple equation approach [18], first integral technique [19], unified approach [20, 21] and so on [22]-[25].

The unified method [20, 21], which is remarkably effective and reliable, is used here to derive and investigate a special class of optical soliton solutions for coupled NHEs. As some published methods, such as the Hirota bilinear method and (G'/G)-expansion technique and so on, have been widely utilized to construct the soliton solutions of NPDEs which lead to complex algebraic computations. The unified method is one among some other simple and great direct algebraic methods which produces a great deal of new soliton solutions in the form of rational, exponential, trigonometric and hyperbolic functions. This simple ansatz also in no need of heavy machinating e.g linearization, perturbation and many expressed there in the literature in other approaches. The simplicity and effectiveness of the employed unified method enable us to develop the accurate closed-form solutions without the inconvenience of more complicated means. The model is transformed to a system of non-linear algebraic equation in the context of series form solution by passing the NPDEs to NODEs employing a wave transformation. Various soliton solutions can be derived by taking any computer algebra system to solve the resultant system. A single travelling wave packet such as a soliton is a pulse that maintains its shape and velocity in a medium without diffusing, and one of these configurations that may maintain itself in the time-evolution of the field is the pulse graph. From the mathematical point of view, the soliton solutions of NPDEs are still significant, since they are much more detailed and

accurate compared with the ordinary solutions. Their natural resilience and strength also allows them to be used useful in many technological and scientific applications. They are very effective to preserve a large amount of concordance and for a sufficient transfer of information as expressiveness for nonlinear systems.

In order to enhance of the phase and the modulated amplitude of continuous waves and to simulate the gradually more compact support of plasmon resonance and photonic devices, the NHEs makes a demand of a very important Shr"odinger-class model. From the physical point of view coupled NHEs describes transverse interactions, transmission of coupled waves and optical solitons' propagation in the field of fiber optics [26]. The associated NHEs are given by [27]:

$$\begin{aligned} iE_t + \frac{E_{xx}}{2} + \chi E_{tt} + \varsigma_1 \left|E^2\right| E + \varsigma_2 E \left|U^2\right| = 0, \\ iU_t + \frac{U_{xx}}{2} + \chi U_{tt} + \varsigma_1 \left|E^2\right| U + \varsigma_2 U \left|U^2\right| = 0, \end{aligned} \tag{1}$$

where i stands for the imaginary unit whereas $E = E(t, s)$ and $U = U(t, s)$ are the envelope fields of the first and the second component, respectively. In above system, Helmholtz nonparaxiality is accounted for by the seconds terms E_{xx} and U_{xx} along with the coefficient $\chi(> 0)$ that represents the level of the nonparaxial parameter and can be modeled as such, while ς_1 and ς_2 are, nonlinearity coefficients, which can, with some stress, be placed in the equation itself. But allowing for a more general class of nonlinearity of mixed (focusing-defocusing) type, (or with focusing and defocusing indices, as those would appear in the focusing case also (ς_1,$\varsigma_2 > 0$) and defocusing case (ς_1,$\varsigma_2 < 0$), respectively. When $\varsigma_1 = \varsigma_2 = \pm 1$, the above system reduces to Helmholtz-Manakov system.

Other investigators have also studied symmetric and asymmetric coupled NHEs before initiating this study. For instance, Tamilselvan et al. constructed and addressed this model through the ansatz technique [28]. Singh et al. utilized exp-function expansion method to arrive at travelling wave solutions for the targeted model [29]. Saha et al. developed chirped gray and anti-dark solutions for coupled NHE with cubic nonlinearity [30]. Finally, by applying the (G'/G)-expansion approach, Alsaud et al. constructed optical soliton solutions for the aimed CNHEs [27]. For the aimed NHEs, this research exploration presents and analyzes new types of optical soliton solutions in the shape of the exponential, hyperbolic, trigonometric and rational functions with the aid of unified approach. The present work is motivated by the ongoing investigations of solitary wave particularly soliton solutions of the model. To reveal as well as visualize the propagation features of the established optical soliton solutions, this study exhibits a set of $3D$, $2D$ and contour plots. These illustrations demonstrate that the generated quasi-periodic type solitons consist of periodic and axial perturbations, leading to optical fractals. Moreover, our implemented unified method is demonstrated to be useful, giving a useful insight on strongly coupled NHE behaviour, increasing the class of optical soliton solutions and suggests applications in nonlinear model control.

Finally, the study of the dynamic behavior of the systems through time series plots, phase space diagrams as well as Hamiltonian analysis has emerged in the recent years as a new field of study. For example, Borhan et al. investigated the bifurcation behaviour, sensitivity analysis and chaotic motions of two (3+1)-dimensional NPDEs such as Jimbo-Miwa equations and Kadomtsev-Petviashvili equation [31]. Hosseini et al. investigated the dynamical system of the generalized Schrödinger equation obtained by Galilean transformation and bifurcation of the governing model using the planar dynamical system theory [32]. In another work, via expressing equation as Hamiltonian system, Qi et al. investigated the bifurcation and phase diagrams of the electrical transmission line model in fractional order and analyzed chaotic behavior and sensitivity of the system [33]. Finally, Hossain et al. performed sensitivity and bifurcation analysis the Hamiltonian amplitude equation [34]. Motivated by recent work about Hamiltonian analysis, we also investigate the bifurcations and chaotic behavior and find that it appears in the dynamical system and get good outcomes concerning fractals and periodicity in the governing system.

The rest of the documentation is organized in the following form: Section 2: Explains the structure and functioning of the hired unified approach, Section 3: Establishes novel plethora optical soliton solutions for coupled NHEs, Section 4: Graphical illustrations of the obtained optical quasi-periodic solitons, Section 5: Presents analysis of the model with regards to bifurcation and chaos theory and the final section presents conclusion of the work.

2. The Working Methodology of Unified Approach

Considering the subsequent general NPDE [20, 21]:

$$M(E, E_t, E_{x_1}, E_{x_2}, EE_{x_1}, \ldots) = 0, \tag{2}$$

where $E = E(t, x_1, x_2, x_3, \ldots, x_k)$. In accordance with the unified approach, (2) is initially transformed to the subsequent NODE with the use of wave transformation of the form $E(t, x_1, x_2, x_3, \ldots, x_k) = \mathfrak{E}(\zeta)$ where ζ:

$$N(\mathfrak{E}, \mathfrak{E}'\mathfrak{E}, \mathfrak{E}', \ldots) = 0, \tag{3}$$

where $\mathfrak{E}' = \frac{d\mathfrak{E}}{d\zeta}$. When applicable, the integrating equation (3) can be invoked to enforce the homogeneous balance condition on the NODE. Next, the close-form solution for the resulting NODE in (3) is then supposed as:

$$\mathfrak{E}(\zeta) = \sum_{j=-P}^{P} \alpha_j (V(\zeta))^j, \tag{4}$$

where $V(\zeta)$ is determined by the following Riccati equation, $\alpha_j (j = -P, ..., P)$ are constants that should be determined by calculation, and $P \in N$ is known as balance number

that is derived from the homogeneous balancing of the largest nonlinearity and the highest-order derivative in (3):

$$V'(\zeta) = (V(\zeta))^2 + \beta. \tag{5}$$

Where $V' = \frac{dV}{d\zeta}$ and β is a real constant. Moreover, corresponding to the values of β, we have the ensuing classes of exact solutions for (5):

Type. 1: Considering $\beta < 0$:

$$V_1(\zeta) = \pm\frac{\sqrt{-\left(\vartheta^2+\kappa^2\right)\beta} - \vartheta\sqrt{-\beta}\cosh\left(2\sqrt{-\beta}\left(\zeta+\xi\right)\right)}{\vartheta\sinh\left(2\sqrt{-\beta}\left(\zeta+\xi\right)\right)+\kappa}, \tag{6}$$

$$V_2(\zeta) = \pm\sqrt{-\beta} + \frac{\mp 2\vartheta\sqrt{-\beta}}{\vartheta+\cosh\left(2\sqrt{-\beta}\left(\zeta+\xi\right)\right)\mp\sinh\left(2\sqrt{-\beta}\left(\zeta+\xi\right)\right)}, \tag{7}$$

$$V_3(\zeta) = \sqrt{-\beta}\tanh\left(\sqrt{-\beta}\left(\zeta+\xi\right)\right), \tag{8}$$

and

$$V_4(\zeta) = \sqrt{-\beta}\coth\left(\sqrt{-\beta}\left(\zeta+\xi\right)\right). \tag{9}$$

Type. 2: Considering $\beta > 0$:

$$V_5(\zeta) = \frac{\pm\sqrt{\left(\vartheta^2-\kappa^2\right)\beta} - \vartheta\sqrt{\beta}\cos\left(2\sqrt{\beta}\left(\zeta+\xi\right)\right)}{\vartheta\sin\left(2\sqrt{\beta}\left(\zeta+\xi\right)\right)+\kappa}, \tag{10}$$

$$V_6(\zeta) = \pm i\sqrt{\beta} + \frac{\mp 2\,i\vartheta\sqrt{\beta}}{\vartheta+\cos\left(2\sqrt{\beta}\left(\zeta+\xi\right)\right)\mp\sin\left(2\sqrt{\beta}\left(\zeta+\xi\right)\right)}, \tag{11}$$

$$V_7(\zeta) = \sqrt{\beta}\tan\left(\sqrt{\beta}\left(\zeta+\xi\right)\right), \tag{12}$$

and

$$V_8(\zeta) = -\sqrt{\beta}\cot\left(\sqrt{\beta}\left(\zeta+\xi\right)\right). \tag{13}$$

Type. 3: Considering $\beta = 0$:

$$V_9(\zeta) = \frac{-1}{\zeta+\xi}. \tag{14}$$

In above solutions $\xi, \vartheta, \kappa \in R$. A system of algebraic equations is then produced when (4) is incorporated into (3) and the coefficients of $V(\zeta)$ are equated to zero. When solved using Maple, this system yields values of $\alpha_j (j = -P, ..., P)$ and other unknown. When substituted these acquired values (along with the solution $V(\zeta)$ of (5))in (4), explicit solutions for (2) are established.

3. Main Results

The proposed unified approach is used in this section of the investigation to establish novel plethora of optical soliton solutions for coupled NHEs in (1). Initially, the ensuing complex transformation is applied to (1):

$$\begin{aligned} &E(t,s) = e^{i\Upsilon}\mathfrak{E}(\zeta), \quad U(t,s) = e^{i\Upsilon}\mathfrak{U}(\zeta), \\ &\zeta = (\mu_3 s - \mu_3\mu_4 t), \quad \Upsilon = (-\mu_1 s + \mu_2 t + \theta). \end{aligned} \tag{15}$$

This transformation yields

$$\begin{aligned} &(-{\mu_3}^2 - 2\chi{\mu_3}^2{\mu_4}^2)\mathfrak{E}'' + ({\mu_1}^2 + 2\mu_2 + 2\chi{\mu_2}^2)\mathfrak{E} + (-2\varsigma_1\mathfrak{E}^3 - 2\varsigma_2\mathfrak{E}\mathfrak{U}^2) = 0, \\ &(2\mu_1\mu_3 + 2\mu_3\mu_4 + 4\chi\mu_2\mu_3\mu_4)\mathfrak{E}' = 0, \end{aligned} \tag{16}$$

from the real component whilst the imaginary part provides:

$$\begin{aligned} &(-{\mu_3}^2 - 2\chi{\mu_3}^2{\mu_4}^2)\mathfrak{U}'' + ({\mu_1}^2 + 2\mu_2 + 2\chi{\mu_2}^2)\mathfrak{U} + (-2\varsigma_1\mathfrak{E}^2\mathfrak{U} - 2\varsigma_2\mathfrak{U}^3) = 0, \\ &(2\mu_1\mu_3 + 2\mu_3\mu_4 + 4\chi\mu_2\mu_3\mu_4)\mathfrak{U}' = 0. \end{aligned} \tag{17}$$

The entire system of NODEs given in (16) and (17) is reduced to the ensuing single NODE when $\mathfrak{U} = \mathfrak{E}$ is considered:

$$\Theta_1\mathfrak{E} + \Theta_2\mathfrak{E}'' + \Theta_3\mathfrak{E}^3 = 0, \tag{18}$$

Also from the imaginary part, we have the following constraint condition:

$$\mu_4 = \frac{-\mu_1}{1 + 2\chi\mu_2}. \tag{19}$$

Also in (18)

$$\begin{aligned} \Theta_1 &= ({\mu_1}^2 + 2\mu_2 + 2\chi{\mu_2}^2), \\ \Theta_2 &= (-{\mu_3}^2 - 2\chi{\mu_3}^2{\mu_4}^2), \\ \Theta_3 &= (-2(\varsigma_1 + \varsigma_2)). \end{aligned}$$

By homogeneously balancing $\mathfrak{E}^3(\zeta)$ with $\mathfrak{E}''(\zeta)$ presented in (18), we get $P = 1$ which suggests the subsequent solution for (18) when substituted in (4):

$$\mathfrak{E}(\zeta) = \sum_{j=-1}^{1} \alpha_j (V(\zeta))^j. \tag{20}$$

Substituting (20) for ζ into (18), combining every term in $V(\zeta)$ in the equal power we obtain expression in $V(\zeta)$. The problem is reduced to the following system of nonlinear algebraic equations when the coefficients are set to zero:

$$-2\,{\mu_3}^2\alpha_1 - 2\,\varsigma_2{\alpha_1}^3 - 2\,\varsigma_1{\alpha_1}^3 - 4\,\frac{\chi\,{\mu_3}^2{\mu_1}^2\alpha_1}{(1 + 2\,\chi\,\mu_2)^2} = 0,$$

$$-6\,\varsigma_2\alpha_0{\alpha_1}^2-6\,\varsigma_1\alpha_0{\alpha_1}^2=0,$$

$$(-6\,\varsigma_1\alpha_{-1}-6\,\varsigma_2\alpha_{-1})\,{\alpha_1}^2+\left(\frac{-4\,\chi\,{\mu_3}^2{\mu_1}^2\beta}{(1+2\,\chi\,\mu_2)^2}-6\,\varsigma_2{\alpha_0}^2-2\,{\mu_3}^2\beta-6\,\varsigma_1{\alpha_0}^2+2\,\chi\,{\mu_2}^2+{\mu_1}^2+2\,\mu_2\right)\alpha_1=0,$$

$$2\,\mu_2\alpha_0-12\,\varsigma_2\alpha_{-1}\alpha_0\alpha_1+{\mu_1}^2\alpha_0-12\,\varsigma_1\alpha_{-1}\alpha_0\alpha_1-2\,\varsigma_2{\alpha_0}^3+2\,\chi\,{\mu_2}^2\alpha_0-2\,\varsigma_1{\alpha_0}^3=0,$$

$$(-6\,\varsigma_2\alpha_1-6\,\varsigma_1\alpha_1)\,{\alpha_{-1}}^2+\left(\frac{-4\,\chi\,{\mu_3}^2{\mu_1}^2\beta}{(1+2\,\chi\,\mu_2)^2}-6\,\varsigma_2{\alpha_0}^2-2\,{\mu_3}^2\beta-6\,\varsigma_1{\alpha_0}^2+2\,\chi\,{\mu_2}^2+{\mu_1}^2+2\,\mu_2\right)\alpha_{-1}=0,$$

$$-6\,\varsigma_2{\alpha_{-1}}^2\alpha_0-6\,\varsigma_1{\alpha_{-1}}^2\alpha_0=0,$$

and

$$-4\,\frac{\chi\,{\mu_3}^2{\mu_1}^2\alpha_{-1}\beta^2}{(1+2\,\chi\,\mu_2)^2}-2\,\varsigma_1{\alpha_{-1}}^3-2\,{\mu_3}^2\alpha_{-1}\beta^2-2\,\varsigma_2{\alpha_{-1}}^3=0.$$

Three (3) families of solutions are obtained by Maple for the resulting problem:
Case. 1

$$\alpha_0=0,\alpha_1=0,\alpha_{-1}=\alpha_{-1},\mu_1=\sqrt{-\frac{-2\,\chi\,{\mu_2}^2-2\,\mu_2+2\,{\mu_3}^2\beta}{4\,{\mu_3}^2\beta\,\chi-1-4\,\chi\,\mu_2-4\,\chi^2{\mu_2}^2}\,(1+2\,\chi\,\mu_2)},\mu_2=\mu_2,$$
$$\mu_3=\mu_3,\chi=\chi,\varsigma_1=\frac{4\,\varsigma_2{\alpha_{-1}}^2\chi^2{\mu_2}^2+4\,\varsigma_2{\alpha_{-1}}^2\chi\,\mu_2-4\,{\mu_3}^2\beta\,\chi\,\varsigma_2{\alpha_{-1}}^2+\varsigma_2{\alpha_{-1}}^2+{\mu_3}^2\beta^2}{{\alpha_{-1}}^2\,(4\,{\mu_3}^2\beta\,\chi-1-4\,\chi\,\mu_2-4\,\chi^2{\mu_2}^2)},\varsigma_2=\varsigma_2. \tag{21}$$

Case. 2

$$\alpha_0=0,\alpha_1=\alpha_1,\alpha_{-1}=0,\mu_1=\sqrt{-\frac{-2\,\chi\,{\mu_2}^2-2\,\mu_2+2\,{\mu_3}^2\beta}{4\,{\mu_3}^2\beta\,\chi-1-4\,\chi\,\mu_2-4\,\chi^2{\mu_2}^2}\,(1+2\,\chi\,\mu_2)},\mu_2=\mu_2,$$
$$\mu_3=\mu_3,\chi=\chi,\varsigma_1=-\frac{-4\,\varsigma_2{\alpha_1}^2\chi^2{\mu_2}^2-4\,\varsigma_2{\alpha_1}^2\chi\,\mu_2+4\,{\mu_3}^2\beta\,\chi\,\varsigma_2{\alpha_1}^2-\varsigma_2{\alpha_1}^2-{\mu_3}^2}{{\alpha_1}^2\,(4\,{\mu_3}^2\beta\,\chi-1-4\,\chi\,\mu_2-4\,\chi^2{\mu_2}^2)},\varsigma_2=\varsigma_2. \tag{22}$$

Case. 3

$$\alpha_0=0,\alpha_1=\alpha_1,\alpha_{-1}=\beta\,\alpha_1,\mu_1=\sqrt{-\frac{2\,\chi\,{\mu_2}^2+2\,\mu_2+4\,{\mu_3}^2\beta}{8\,{\mu_3}^2\beta\,\chi+1+4\,\chi\,\mu_2+4\,\chi^2{\mu_2}^2}\,(1+2\,\chi\,\mu_2)},\mu_2=\mu_2,$$
$$\mu_3=\mu_3,\chi=\chi,\varsigma_1=-\frac{4\,\varsigma_2{\alpha_1}^2\chi^2{\mu_2}^2+4\,\varsigma_2{\alpha_1}^2\chi\,\mu_2+8\,{\mu_3}^2\beta\,\chi\,\varsigma_2{\alpha_1}^2+\varsigma_2{\alpha_1}^2+{\mu_3}^2}{{\alpha_1}^2\,(8\,{\mu_3}^2\beta\,\chi+1+4\,\chi\,\mu_2+4\,\chi^2{\mu_2}^2)},\varsigma_2=\varsigma_2. \tag{23}$$

Using **Case. 1** together with the solution to (4), (15) and (20), we establish the subsequent novel class of solutions for coupled NHEs stated in (1):
Type. 1.1 Considering $\beta<0$:

$$E_{1,1}(t,s)=U_{1,1}(t,s)=e^{i\Upsilon}\left(\frac{\alpha_{-1}\left(\vartheta\sinh\left(2\sqrt{-\beta}\,(\zeta+\xi)\right)+\kappa\right)}{\sqrt{-\left(\vartheta^2+\kappa^2\right)\beta}-\vartheta\sqrt{-\beta}\cosh\left(2\sqrt{-\beta}\,(\zeta+\xi)\right)}\right), \tag{24}$$

$$E_{1,2}(t,s)=U_{1,2}(t,s)=e^{i\Upsilon}\left(\alpha_{-1}\left(\sqrt{-\beta}-2\,\frac{\vartheta\sqrt{-\beta}}{\vartheta+\cosh\left(2\sqrt{-\beta}\,(\zeta+\xi)\right)-\sinh\left(2\sqrt{-\beta}\,(\zeta+\xi)\right)}\right)^{-1}\right), \tag{25}$$

$$E_{1,3}(t,s)=U_{1,3}(t,s)=e^{i\Upsilon}\left(\frac{\alpha_{-1}}{\sqrt{-\beta}\tanh\left(\sqrt{-\beta}\,(\zeta+\xi)\right)}\right), \tag{26}$$

and

$$E_{1,4}(t,s)=U_{1,4}(t,s)=e^{i\Upsilon}\left(\frac{\alpha_{-1}}{\sqrt{-\beta}\coth\left(\sqrt{-\beta}\,(\zeta+\xi)\right)}\right). \tag{27}$$

Type. 1.2 Considering $\beta>0$:

$$E_{1,5}(t,s)=U_{1,5}(t,s)=e^{i\Upsilon}\left(\frac{\alpha_{-1}\left(\vartheta\sin\left(2\sqrt{\beta}\,(\zeta+\xi)\right)+\kappa\right)}{\sqrt{(\vartheta^2-\kappa^2)\,\beta}-\vartheta\sqrt{\beta}\cos\left(2\sqrt{\beta}\,(\zeta+\xi)\right)}\right), \tag{28}$$

$$E_{1,6}(t,s)=U_{1,6}(t,s)=e^{i\Upsilon}\left(\alpha_{-1}\left(i\sqrt{\beta}-\frac{2\,i\vartheta\sqrt{\beta}}{\vartheta+\cos\left(2\sqrt{\beta}\,(\zeta+\xi)\right)-\sin\left(2\sqrt{\beta}\,(\zeta+\xi)\right)}\right)^{-1}\right), \tag{29}$$

$$E_{1,7}(t,s)=U_{1,7}(t,s)=e^{i\Upsilon}\left(\frac{\alpha_{-1}}{\sqrt{\beta}\tan\left(\sqrt{\beta}\,(\zeta+\xi)\right)}\right), \tag{30}$$

and

$$E_{1,8}(t,s)=U_{1,8}(t,s)=e^{i\Upsilon}\left(-\frac{\alpha_{-1}}{\sqrt{\beta}\cot\left(\sqrt{\beta}\,(\zeta+\xi)\right)}\right). \tag{31}$$

Type. 1.3 Considering $\beta=0$:

$$E_{1,9}(t,s)=U_{1,9}(t,s)=e^{i\Upsilon}\left(-\alpha_{-1}\,(\zeta+\xi)\right). \tag{32}$$

Where $\zeta=\mu_3(s-(\frac{-\sqrt{-\frac{-2\,\chi\,{\mu_2}^2-2\,\mu_2+2\,{\mu_3}^2\beta}{4\,{\mu_3}^2\beta\,\chi-1-4\,\chi\,\mu_2-4\,\chi^2{\mu_2}^2}}(1+2\,\chi\,\mu_2)}{1+2\chi\mu_2})t)$,
$\Upsilon=(-\sqrt{-\frac{-2\,\chi\,{\mu_2}^2-2\,\mu_2+2\,{\mu_3}^2\beta}{4\,{\mu_3}^2\beta\,\chi-1-4\,\chi\,\mu_2-4\,\chi^2{\mu_2}^2}}\,(1+2\,\chi\,\mu_2)s+\mu_2 t+\theta)$.
Using **Case. 2** together with the solution to (4), (15) and (20), we establish the subsequent novel class of solutions for coupled NHEs stated in (1):
Type. 2.1 Considering $\beta<0$:

$$E_{2,1}(t,s)=U_{2,1}(t,s)=e^{i\Upsilon}\left(\frac{\alpha_1\left(\sqrt{-(\vartheta^2+\kappa^2)\,\beta}-\vartheta\sqrt{-\beta}\cosh\left(2\sqrt{-\beta}\,(\zeta+\xi)\right)\right)}{\vartheta\sinh\left(2\sqrt{-\beta}\,(\zeta+\xi)\right)+\kappa}\right), \tag{33}$$

$$E_{2,2}(t,s) = U_{2,2}(t,s) = e^{i\Upsilon}\left(\alpha_1\left(\sqrt{-\beta} - 2\,\frac{\vartheta\sqrt{-\beta}}{\vartheta + \cosh\left(2\sqrt{-\beta}\,(\zeta+\xi)\right) - \sinh\left(2\sqrt{-\beta}\,(\zeta+\xi)\right)}\right)\right), \tag{34}$$

$$E_{2,3}(t,s) = U_{2,3}(t,s) = e^{i\Upsilon}\left(\alpha_1\sqrt{-\beta}\tanh\left(\sqrt{-\beta}\,(\zeta+\xi)\right)\right), \tag{35}$$

and

$$E_{2,4}(t,s) = U_{2,4}(t,s) = e^{i\Upsilon}\left(\alpha_1\sqrt{-\beta}\coth\left(\sqrt{-\beta}\,(\zeta+\xi)\right)\right). \tag{36}$$

Type. 2.2 Considering $\beta > 0$:

$$E_{2,5}(t,s) = U_{2,5}(t,s) = e^{i\Upsilon}\left(\frac{\alpha_1\left(\sqrt{(\vartheta^2-\kappa^2)\,\beta} - \vartheta\sqrt{\beta}\cos\left(2\sqrt{\beta}\,(\zeta+\xi)\right)\right)}{\vartheta\sin\left(2\sqrt{\beta}\,(\zeta+\xi)\right) + \kappa}\right), \tag{37}$$

$$E_{2,6}(t,s) = U_{2,6}(t,s) = e^{i\Upsilon}\left(\alpha_1\left(i\sqrt{\beta} - \frac{2\,i\vartheta\sqrt{\beta}}{\vartheta + \cos\left(2\sqrt{\beta}\,(\zeta+\xi)\right) - \sin\left(2\sqrt{\beta}\,(\zeta+\xi)\right)}\right)\right), \tag{38}$$

$$E_{2,7}(t,s) = U_{2,7}(t,s) = e^{i\Upsilon}\left(\alpha_1\sqrt{\beta}\tan\left(\sqrt{\beta}\,(\zeta+\xi)\right)\right), \tag{39}$$

and

$$E_{2,8}(t,s) = U_{2,8}(t,s) = e^{i\Upsilon}\left(-\alpha_1\sqrt{\beta}\cot\left(\sqrt{\beta}\,(\zeta+\xi)\right)\right). \tag{40}$$

Type. 2.3 Considering $\beta = 0$:

$$E_{2,9}(t,s) = U_{2,9}(t,s) = e^{i\Upsilon}\left(-\frac{\alpha_1}{\zeta+\xi}\right). \tag{41}$$

Where $\zeta = \mu_3(s - (\frac{-\sqrt{-\frac{-2\,\chi\,{\mu_2}^2-2\,\mu_2+2\,{\mu_3}^2\beta}{4\,{\mu_3}^2\beta\,\chi-1-4\,\chi\,\mu_2-4\,\chi^2{\mu_2}^2}}(1+2\,\chi\,\mu_2)}{1+2\chi\mu_2})t)$,
$\Upsilon = (-\sqrt{-\frac{-2\,\chi\,{\mu_2}^2-2\,\mu_2+2\,{\mu_3}^2\beta}{4\,{\mu_3}^2\beta\,\chi-1-4\,\chi\,\mu_2-4\,\chi^2{\mu_2}^2}}\,(1+2\,\chi\,\mu_2)s + \mu_2 t + \theta)$.
Using **Case. 2** together with the solution to (4), (15) and (20), we establish the subsequent novel class of solutions for coupled NHEs stated in (1):
Type. 3.1 Considering $\beta < 0$:

$$\begin{aligned} E_{3,1}(t,s) = U_{3,1}(t,s) = e^{i\Upsilon}\Bigg(&\frac{\beta\,\alpha_1\left(\vartheta\sinh\left(2\sqrt{-\beta}\,(\zeta+\xi)\right)+\kappa\right)}{\sqrt{-\left(\vartheta^2+\kappa^2\right)\beta} - \vartheta\sqrt{-\beta}\cosh\left(2\sqrt{-\beta}\,(\zeta+\xi)\right)} \\ &+ \frac{\alpha_1\left(\sqrt{-\left(\vartheta^2+\kappa^2\right)\beta} - \vartheta\sqrt{-\beta}\cosh\left(2\sqrt{-\beta}\,(\zeta+\xi)\right)\right)}{\vartheta\sinh\left(2\sqrt{-\beta}\,(\zeta+\xi)\right)+\kappa}\Bigg), \end{aligned} \tag{42}$$

$$E_{3,2}(t,s) = U_{3,2}(t,s) = e^{i\Upsilon}\left(\beta\,\alpha_1\left(\sqrt{-\beta} - 2\,\frac{\vartheta\sqrt{-\beta}}{\vartheta + \cosh\left(2\sqrt{-\beta}\,(\zeta+\xi)\right) - \sinh\left(2\sqrt{-\beta}\,(\zeta+\xi)\right)}\right)^{-1} + \alpha_1\left(\sqrt{-\beta} - 2\,\frac{\vartheta\sqrt{-\beta}}{\vartheta + \cosh\left(2\sqrt{-\beta}\,(\zeta+\xi)\right) - \sinh\left(2\sqrt{-\beta}\,(\zeta+\xi)\right)}\right)\right), \tag{43}$$

$$E_{3,3}(t,s) = U_{3,3}(t,s) = e^{i\Upsilon}\left(\frac{\beta\,\alpha_1}{\sqrt{-\beta}\tanh\left(\sqrt{-\beta}\,(\zeta+\xi)\right)} + \alpha_1\sqrt{-\beta}\tanh\left(\sqrt{-\beta}\,(\zeta+\xi)\right)\right), \tag{44}$$

and

$$E_{3,4}(t,s) = U_{3,4}(t,s) = e^{i\Upsilon}\left(\frac{\beta\,\alpha_1}{\sqrt{-\beta}\coth\left(\sqrt{-\beta}\,(\zeta+\xi)\right)} + \alpha_1\sqrt{-\beta}\coth\left(\sqrt{-\beta}\,(\zeta+\xi)\right)\right). \tag{45}$$

Type. 3.2 Considering $\beta > 0$:

$$E_{3,5}(t,s) = U_{3,5}(t,s) = e^{i\Upsilon}\left(\frac{\beta\,\alpha_1\left(\vartheta\sin\left(2\sqrt{\beta}\,(\zeta+\xi)\right) + \kappa\right)}{\sqrt{(\vartheta^2-\kappa^2)\,\beta} - \vartheta\sqrt{\beta}\cos\left(2\sqrt{\beta}\,(\zeta+\xi)\right)} + \frac{\alpha_1\left(\sqrt{(\vartheta^2-\kappa^2)\,\beta} - \vartheta\sqrt{\beta}\cos\left(2\sqrt{\beta}\,(\zeta+\xi)\right)\right)}{\vartheta\sin\left(2\sqrt{\beta}\,(\zeta+\xi)\right) + \kappa}\right), \tag{46}$$

$$E_{3,6}(t,s) = U_{3,6}(t,s) = e^{i\Upsilon}\left(\beta\,\alpha_1\left(i\sqrt{\beta} - \frac{2\,i\vartheta\sqrt{\beta}}{\vartheta + \cos\left(2\sqrt{\beta}\,(\zeta+\xi)\right) - \sin\left(2\sqrt{\beta}\,(\zeta+\xi)\right)}\right)^{-1} + \alpha_1\left(i\sqrt{\beta} - \frac{2\,i\vartheta\sqrt{\beta}}{\vartheta + \cos\left(2\sqrt{\beta}\,(\zeta+\xi)\right) - \sin\left(2\sqrt{\beta}\,(\zeta+\xi)\right)}\right)\right), \tag{47}$$

$$E_{3,7}(t,s) = U_{3,7}(t,s) = e^{i\Upsilon}\left(\frac{\alpha_1\sqrt{\beta}}{\tan\left(\sqrt{\beta}\,(\zeta+\xi)\right)} + \alpha_1\sqrt{\beta}\tan\left(\sqrt{\beta}\,(\zeta+\xi)\right)\right), \tag{48}$$

and

$$E_{3,8}(t,s) = U_{3,8}(t,s) = e^{i\Upsilon}\left(-\frac{\alpha_1\sqrt{\beta}}{\cot\left(\sqrt{\beta}\,(\zeta+\xi)\right)} - \alpha_1\sqrt{\beta}\cot\left(\sqrt{\beta}\,(\zeta+\xi)\right)\right). \tag{49}$$

Type. 3.3 Considering $\beta = 0$:

$$E_{3,9}(t,s) = U_{3,9}(t,s) = e^{i\Upsilon}\left(-\frac{\alpha_1}{\zeta+\xi}\right). \tag{50}$$

Where $\zeta = \mu_3(s - (\frac{-\sqrt{-\frac{2\chi{\mu_2}^2+2\mu_2+4{\mu_3}^2\beta}{8{\mu_3}^2\beta\chi+1+4\chi\mu_2+4\chi^2{\mu_2}^2}}(1+2\chi\mu_2)}{1+2\chi\mu_2})t)$,
$\Upsilon = (-\sqrt{-\frac{2\chi{\mu_2}^2+2\mu_2+4{\mu_3}^2\beta}{8{\mu_3}^2\beta\chi+1+4\chi\mu_2+4\chi^2{\mu_2}^2}}\,(1+2\chi\mu_2)s + \mu_2 t + \theta)$.

4. Graphs and Discussion

In this parts of this study, the established optical soliton solutions are shown and discussed graphically that were observed in the model. We have extracted and visualized wave dynamics of optical solitons in 2D, 3D and contour forms with the help of unified technique. These concepts are essential to understand the behavior of connected physical processes. Optical pulse theory is expected to be greatly enriched from optical soliton solutions generated. It was also demonstrated that the optical quasi-periodic solitons corresponding to the coupled NHEs have been formally, visualized through the chaotic perturbation that are axial-periodic perturbations.

The representations also exhibited the existence of the axially-periodic perturbing phenomena in the generated solitons which led to the formation of fractals. These waveforms have the celebrated property that after scattering or interacting with other identical waveforms they have a tendency to spontaneously repair themselves and settle down to be stable. The resultant soliton structures in the NHEs are concrete with respect to the advanced optical technologies. In optical fiber communication systems, solitons exhibit themselves as the forces to neutralize nonlinearity and dispersion, being a core constituent of long-distance and high-capacity signal transport. Fractal soliton profiles, induced by periodic and axial perturbations, demonstrate their intimate relation to localization of light in the fiber optic and to fractal generation of optical fields, which can be useful for designing optical sensors with sensitivity limit extended down to the level of single atoms and for fabrication of optical lattices.

The found quasi-periodic solitons can also be used for all optical reshaping and buffering of signals which is important for all optical computing.

New trends in soliton-theory has created an interesting possibility for new mathematical topics, such as the so called fractal soliton theory [35]-[37] which is the complex relationships between solitons and fractals. A fractal solitary wave is a stable localized wave packet with a simultaneous fractal and a solitonic structure. These results can be connected to solitons and geometric fractals to understand nonlinear phenomena in physics, engineering, biology [38]-[40]. Fractal solitons are important tools when addressing chaos theory since a special feature allows us to understand the dynamics and the stability of chaotic systems. Relating the attention attracted by research on fractal soliton in recent mathematical enterprises of physical interests will generate some new thinking with respect to theoretical and potential mathematics.

Figure. 1 reveals the formation of fractal structure due to the propagation of quasi-

periodic type optical soliton represented by $E_{1,1}(t,s)$ described in (24) for $\mu_2 = 0.005, \mu_3 = 0.002, \beta = -1, \alpha_{-1} = 2, \vartheta = 25, \kappa = 3, \xi = 1, \chi = 1, \theta = 0.5$. Moreover, the 2D plots of the real and imaginary parts of the solution are displayed for $s = 0$.

Figure. 2 reveals the formation of fractal structure due to the propagation of quasi-periodic type optical soliton represented by $E_{1,3}(t,s)$ described in (26) for $\mu_2 = 0.0015, \mu_3 = 0.0025, \beta = -4, \alpha_{-1} = 5, \vartheta = 4, \kappa = 1, \xi = 2, \chi = 3, \theta = 1$. Moreover, the 2D plots of the real and imaginary parts of the solution are displayed for $s = 10$.

Figure. 3 reveals the formation of fractal structure due to the propagation of quasi-periodic type optical soliton represented by $E_{1,5}(t,s)$ described in (28) for $\mu_2 = 0.0075, \mu_3 = 0.0015, \beta = 5, \alpha_{-1} = 2, \vartheta = 3, \kappa = 2, \xi = 1, \chi = 2, \theta = 5$. Moreover, the 2D plots of the real and imaginary parts of the solution are displayed for $s = 50$.

Figure. 4 reveals the formation of fractal structure due to the propagation of quasi-periodic type optical soliton represented by $E_{2,2}(t,s)$ described in (34) for $\mu_2 = 0.0035, \mu_3 = 0.0055, \beta = -3, \alpha_1 = 1, \vartheta = 4, \kappa = 2, \xi = 1, \chi = 3, \theta = 5$. Moreover, the 2D plots of the real and imaginary parts of the solution are displayed for $s = 50$.

Figure. 5 reveals the formation of fractal structure due to the propagation of quasi-periodic type optical soliton represented by $E_{2,6}(t,s)$ described in (38) for $\mu_2 = 0.0025, \mu_3 = 0.0095, \beta = 9, \alpha_1 = 10, \vartheta = 10, \kappa = 1, \xi = 10, \chi = 5, \theta = 10$. Moreover, the 2D plots of the real and imaginary parts of the solution are displayed for $s = 100$.

Figure. 6 reveals the formation of fractal structure due to the propagation of quasi-periodic type optical soliton represented by $E_{2,9}(t,s)$ described in (41) for $\mu_2 = 0.00885, \mu_3 = 0.00775, \beta = 0, \alpha_1 = 5, \vartheta = 9, \kappa = 5, \xi = 20, \chi = 10, \theta = 50$. Moreover, the 2D plots of the real and imaginary parts of the solution are displayed for $s = 10$.

Figure. 7 reveals the formation of fractal structure due to the propagation of quasi-periodic type optical soliton represented by $E_{3,1}(t,s)$ described in (42) for $\mu_2 = 0.0005, \mu_3 = 0.001, \beta = -25, \alpha_1 = 2, \vartheta = 8, \kappa = 2, \xi = 1, \chi = 1, \theta = 10$. Moreover, the 2D plots of the real and imaginary parts of the solution are displayed for $s = 50$.

Figure. 8 reveals the formation of fractal structure due to the propagation of quasi-periodic type optical soliton represented by $E_{3,4}(t,s)$ described in (45) for $\mu_2 = 0.015, \mu_3 = 0.031, \beta = -1, \alpha_1 = 1, \vartheta = 5, \kappa = 1, \xi = 2, \chi = 0.5, \theta = 5$. Moreover, the 2D plots of the real and imaginary parts of the solution are displayed for $s = 0$.

Figure. 9 reveals the formation of fractal structure due to the propagation of quasi-periodic type optical soliton represented by $E_{3,8}(t,s)$ described in (49) for $\mu_2 = 0.005, \mu_3 = 0.001, \beta = 4, \alpha_1 = 2, \vartheta = 6, \kappa = 5, \xi = 1, \chi = 1, \theta = 2$. Moreover, the 2D plots of the real and imaginary parts of the solution are displayed for $s = 10$.

Figure. 10 reveals the formation of fractal structure due to the propagation of quasi-periodic type optical soliton represented by $E_{3,9}(t,s)$ described in (50) for $\mu_2 = 0.125, \mu_3 = 0.525, \beta = 0, \alpha_1 = 5, \vartheta = 1, \kappa = 0, \xi = 2, \chi = 5, \theta = 2$. Moreover, the 2D plots of the real and imaginary parts of the solution are displayed for $s = 10$.

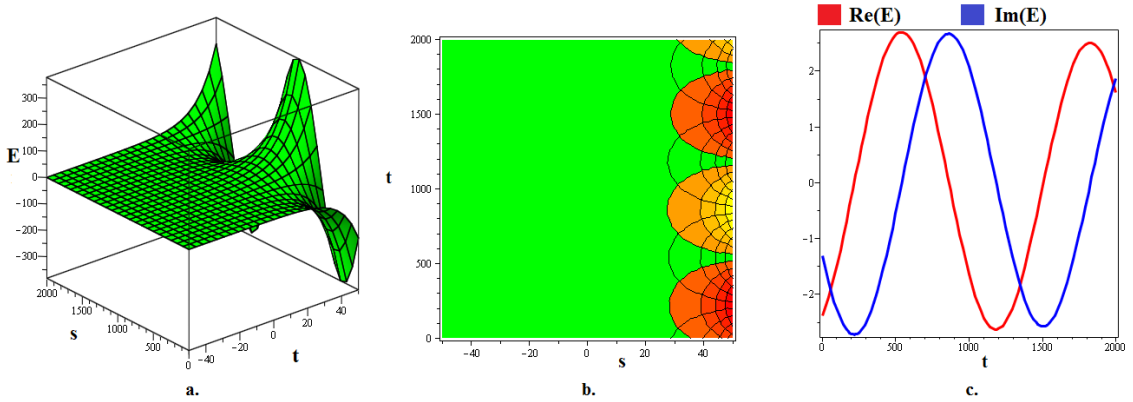

Figure 1: Propagation of quasi-periodic type optical soliton represented by $E_{1,1}(t,s)$ described in (24) for $\mu_2 = 0.005, \mu_3 = 0.002, \beta = -1, \alpha_{-1} = 2, \vartheta = 25, \kappa = 3, \xi = 1, \chi = 1, \theta = 0.5$. Moreover, the 2D plots of the real and imaginary parts of the solution are displayed for $s = 0$.

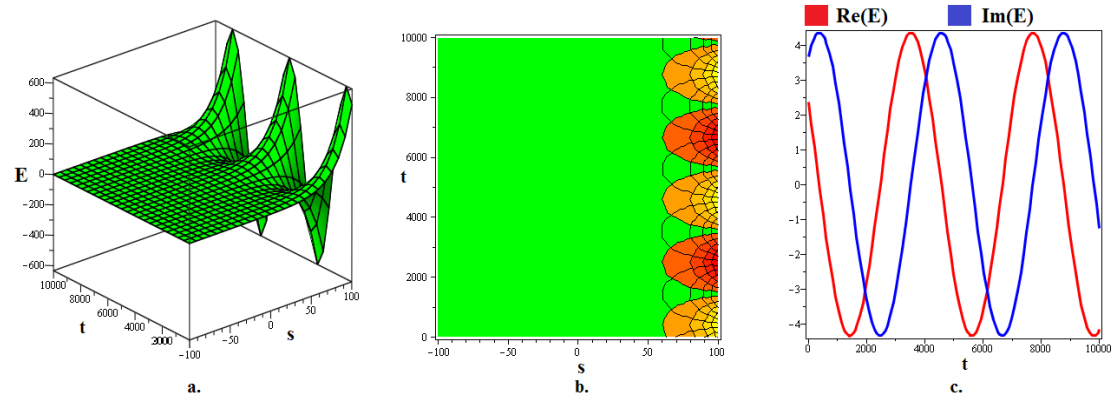

Figure 2: Propagation of quasi-periodic type optical soliton represented by $E_{1,3}(t,s)$ described in (26) for $\mu_2 = 0.0015, \mu_3 = 0.0025, \beta = -4, \alpha_{-1} = 5, \vartheta = 4, \kappa = 1, \xi = 2, \chi = 3, \theta = 1$. Moreover, the 2D plots of the real and imaginary parts of the solution are displayed for $s = 10$.

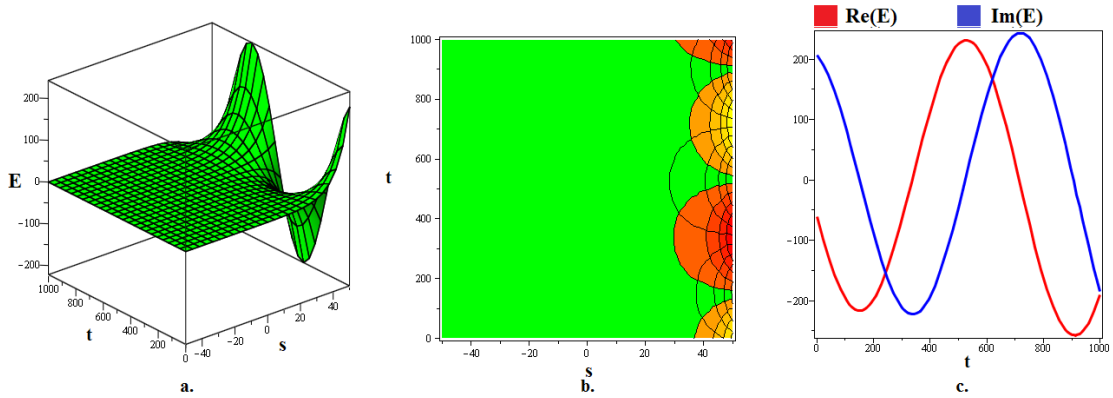

Figure 3: Propagation of quasi-periodic type optical soliton represented by $E_{1,5}(t,s)$ described in (28) for $\mu_2 = 0.0075, \mu_3 = 0.0015, \beta = 5, \alpha_{-1} = 2, \vartheta = 3, \kappa = 2, \xi = 1, \chi = 2, \theta = 5$. Moreover, the 2D plots of the real and imaginary parts of the solution are displayed for $s = 50$.

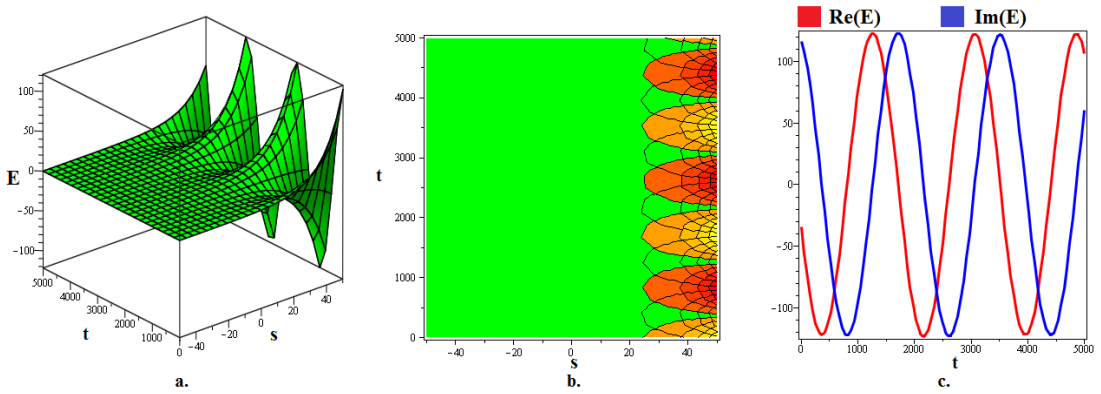

Figure 4: Propagation of quasi-periodic type optical soliton represented by $E_{2,2}(t,s)$ described in (34) for $\mu_2 = 0.0035, \mu_3 = 0.0055, \beta = -3, \alpha_1 = 1, \vartheta = 4, \kappa = 2, \xi = 1, \chi = 3, \theta = 5$. Moreover, the 2D plots of the real and imaginary parts of the solution are displayed for $s = 50$.

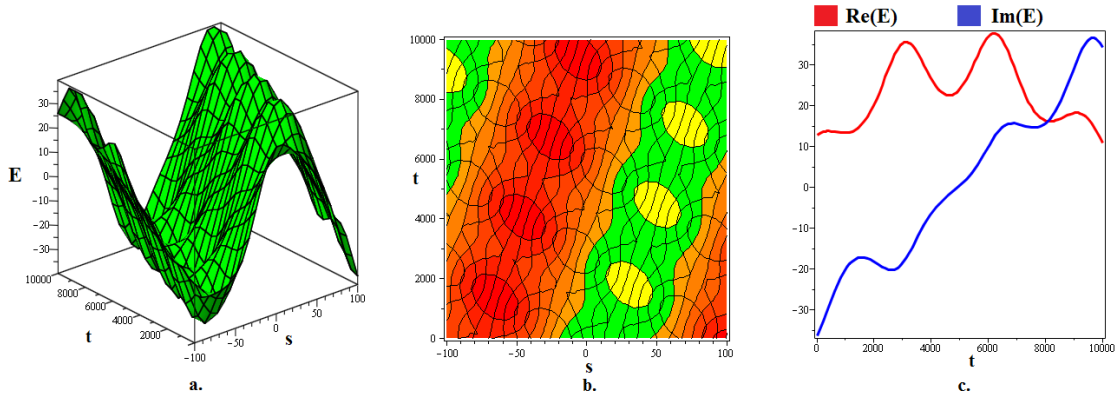

Figure 5: Propagation of quasi-periodic type optical soliton represented by $E_{2,6}(t,s)$ described in (38) for $\mu_2 = 0.0025, \mu_3 = 0.0095, \beta = 9, \alpha_1 = 10, \vartheta = 10, \kappa = 1, \xi = 10, \chi = 5, \theta = 10$. Moreover, the 2D plots of the real and imaginary parts of the solution are displayed for $s = 100$.

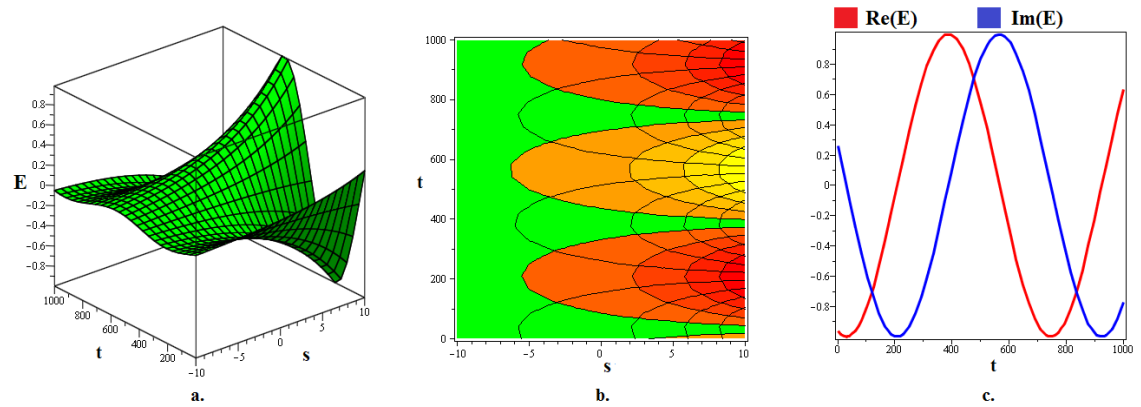

Figure 6: Propagation of quasi-periodic type optical soliton represented by $E_{2,9}(t,s)$ described in (41) for $\mu_2 = 0.00885, \mu_3 = 0.00775, \beta = 0, \alpha_1 = 5, \vartheta = 9, \kappa = 5, \xi = 20, \chi = 10, \theta = 50$. Moreover, the 2D plots of the real and imaginary parts of the solution are displayed for $s = 10$.

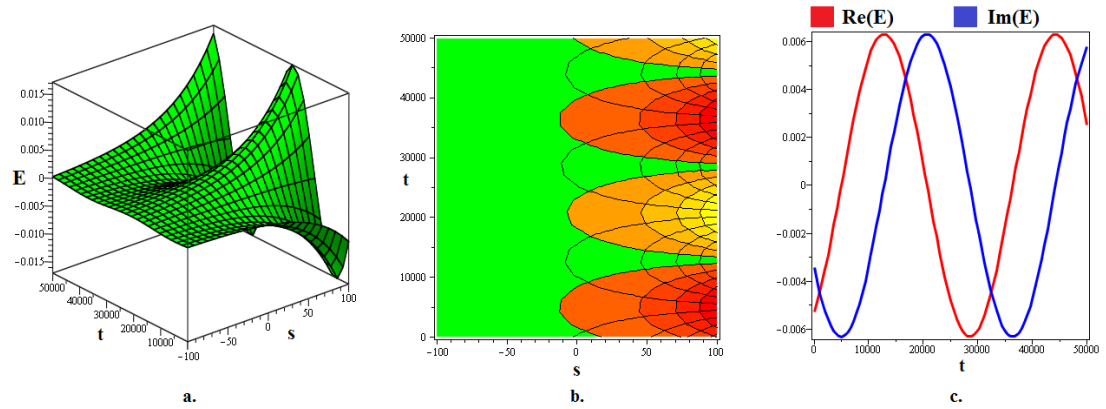

Figure 7: Propagation of quasi-periodic type optical soliton represented by $E_{3,1}(t,s)$ described in (42) for $\mu_2 = 0.0005, \mu_3 = 0.001, \beta = -25, \alpha_1 = 2, \vartheta = 8, \kappa = 2, \xi = 1, \chi = 1, \theta = 10$. Moreover, the 2D plots of the real and imaginary parts of the solution are displayed for $s = 50$.

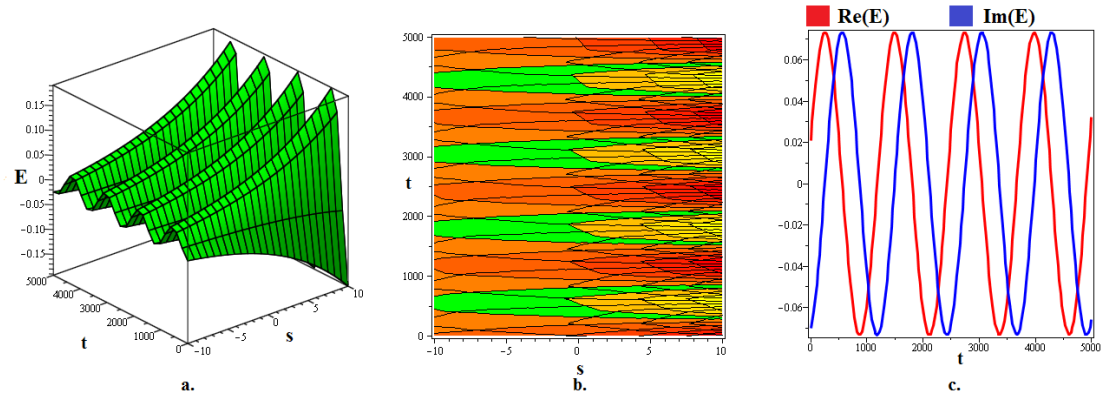

Figure 8: Propagation of quasi-periodic type optical soliton represented by $E_{3,4}(t,s)$ described in (45) for $\mu_2 = 0.015, \mu_3 = 0.031, \beta = -1, \alpha_1 = 1, \vartheta = 5, \kappa = 1, \xi = 2, \chi = 0.5, \theta = 5$. Moreover, the 2D plots of the real and imaginary parts of the solution are displayed for $s = 0$.

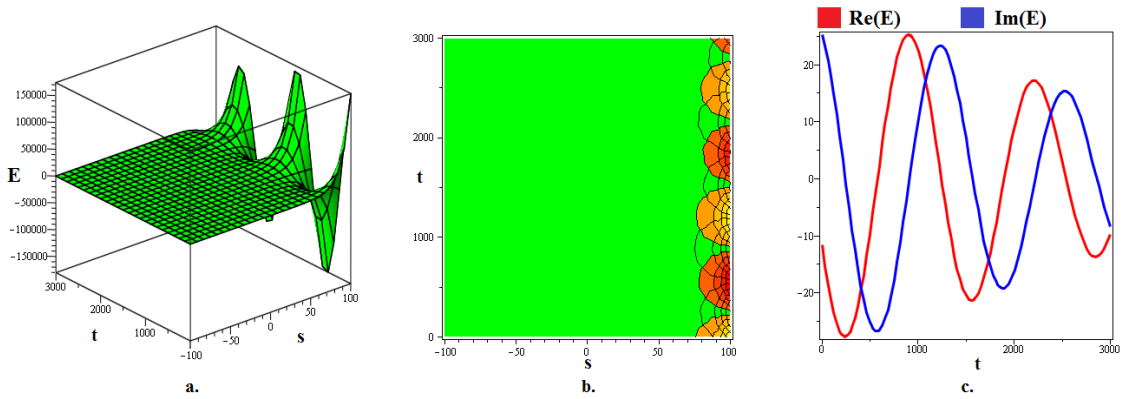

Figure 9: Propagation of quasi-periodic type optical soliton represented by $E_{3,8}(t,s)$ described in (49) for $\mu_2 = 0.005, \mu_3 = 0.001, \beta = 4, \alpha_1 = 2, \vartheta = 6, \kappa = 5, \xi = 1, \chi = 1, \theta = 2$. Moreover, the 2D plots of the real and imaginary parts of the solution are displayed for $s = 10$.

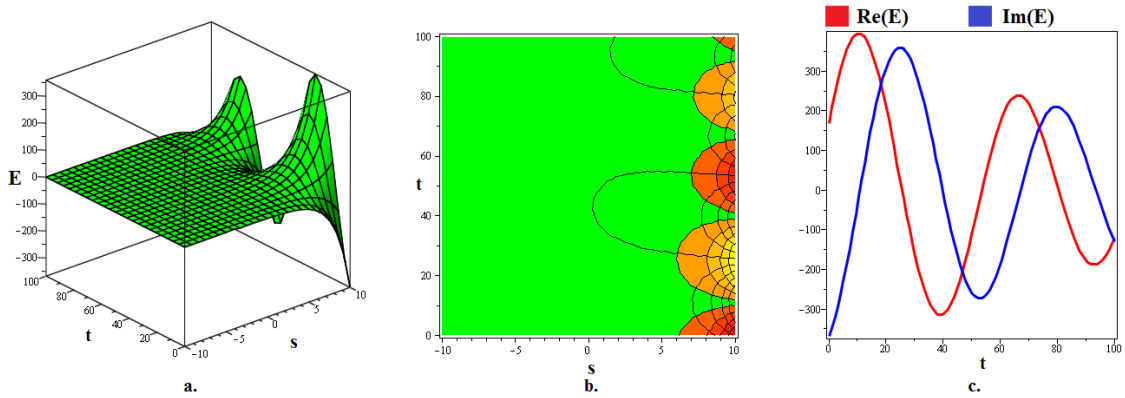

Figure 10: Propagation of quasi-periodic type optical soliton represented by $E_{3,9}(t,s)$ described in (50) for $\mu_2 = 0.125, \mu_3 = 0.525, \beta = 0, \alpha_1 = 5, \vartheta = 1, \kappa = 0, \xi = 2, \chi = 5, \theta = 2$. Moreover, the 2D plots of the real and imaginary parts of the solution are displayed for $s = 10$.

5. Phase Portraits and Time-Series Evaluation

This section provides and evaluates phase portraits of the planner system and the time series plots of the perturbed system using the notion of the Hamiltonian analysis.

5.1. Phase Portraits and Bifurcation Analysis

Using the the notion of the bifurcation theory, we get the subsequent planner system of (9)

$$\begin{aligned} &\mathfrak{E}(\zeta) = G(\zeta) \\ &z(H(\zeta), G(\zeta)) = G'(\zeta) = H(\zeta), \\ &r(H(\zeta), G(\zeta)) = H(\zeta)' = -\frac{\Theta_1}{\Theta_2} G(\zeta) - \frac{\Theta_2}{\Theta_2} G(\zeta)^3, \end{aligned} \tag{51}$$

where

$$\begin{aligned} \Theta_1 &= ({\mu_1}^2 + 2\mu_2 + 2\chi {\mu_2}^2), \\ \Theta_2 &= (-{\mu_3}^2 - 2\chi {\mu_3}^2 {\mu_4}^2), \\ \Theta_3 &= (-2(\varsigma_1 + \varsigma_2)). \end{aligned}$$

Under a given integral, this system displays the following Hamiltonian:

$$Ham(H(\zeta), G(\zeta)) = \frac{H(\zeta)^2}{2} + \frac{\Theta_1}{2\Theta_2} G(\zeta)^2 + \frac{\Theta_2}{4\Theta_2} G(\zeta)^4. \tag{52}$$

We get three equilibria: $(0,0)$, $(R_1,0)$ and $(R_2,0)$ for the planner system where R_1 and R_2 are given below:

$$R_1 = \sqrt{-\frac{\Theta_1}{\Theta_3}}, \quad R_2 = -\sqrt{-\frac{\Theta_1}{\Theta_3}}. \tag{53}$$

Furthermore, according to the Jacobian matrix:

$$J = \begin{bmatrix} \frac{\partial z}{\partial G(\zeta)} & \frac{\partial z}{\partial H(\zeta)} \\ \frac{\partial r}{\partial G(\zeta)} & \frac{\partial r}{\partial H(\zeta)} \end{bmatrix}, \tag{54}$$

The Jacobian of the system is:

$$|J(H(\zeta), G(\zeta))| = \frac{3\Theta_3}{\Theta_2} G(\zeta)^2 + \frac{\Theta_1}{\Theta_2}. \tag{55}$$

An equilibrium point is a saddle or a center based on the value of $|J(H(\zeta), G(\zeta))|$ i.e., an equilibrium point is a saddle for $|J(H(\zeta), G(\zeta))|0$, and transportation if $|J(H(\zeta), G(\zeta))| = 0$. We show next some phase portraits of the planner dynamical system as function of the parameters by selecting different values for them:

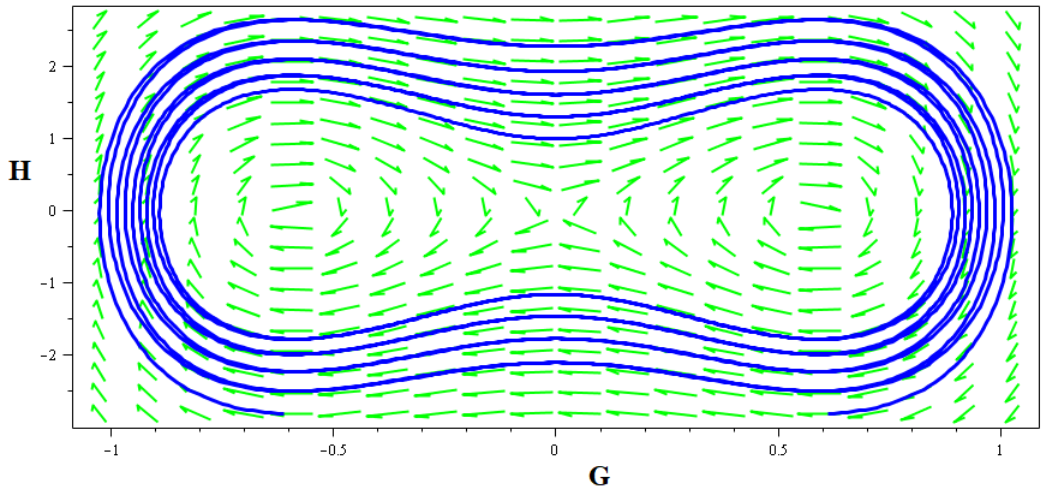

Figure 11: The visualization of phase portrait for (51) at $\mu_1 = 0.10, \mu_2 = 0.20, \mu_3 = 0.20, \chi = 0.10, \varsigma_1 = 0.30, \varsigma_2 = 0.30$.

Remarks: Considering $\Theta_1/\Theta_2 < 0$, according to the phase portrait of planner dynamical system in Fig. (11), we obtain the homoclinic loop with centers $(R_1, 0)$, $(R_2, 0)$ and saddle point $(0, 0)$. Thus, the system seems to shuttle periodically in the state variable coordinate system $[G(\zeta),\ H(\zeta)]$. This can be interpreted to be a regular, dynamic process, caused by mutual emergence of different phases of soliton and exchange of energy. Likewise, the phase portrait of planner dynamical system in the case of $\Theta_1/\Theta_2 > 0$ has been illustrated in Fig. 12, showing a closed circle centered at $(0, 0)$, implying that the system supports a periodic soliton. Closed paths can appear in phase portrait when there is confined or restricted periodic motion. Which indicates the presence of solitonic cycles, where the energy of wave is confined in a repeating cycle without being dissipated rather than fading away or spreading indefinitely.

5.2. The Perturbed System and Time-Series Plots Evaluation

This section presents the time series plots evaluation of the perturbed system for (9). The planner system in (51) is perturbed by adding the periodic term to it for disturbing the periodic behaviour of the system using the Gillion transformation. The perturbed dynamical system for (9) with a periodic external forcing can be expressed as:

$$\begin{aligned} z(H(\zeta), G(\zeta)) &= G(\zeta)' = H(\zeta), \\ y(H(\zeta), G(\zeta)) &= H(\zeta)' = -\frac{\Theta_1}{\Theta_2} G(\zeta) - \frac{\Theta_2}{\Theta_2} G(\zeta)^3 + k_0 \sin(\gamma\zeta). \end{aligned} \tag{56}$$

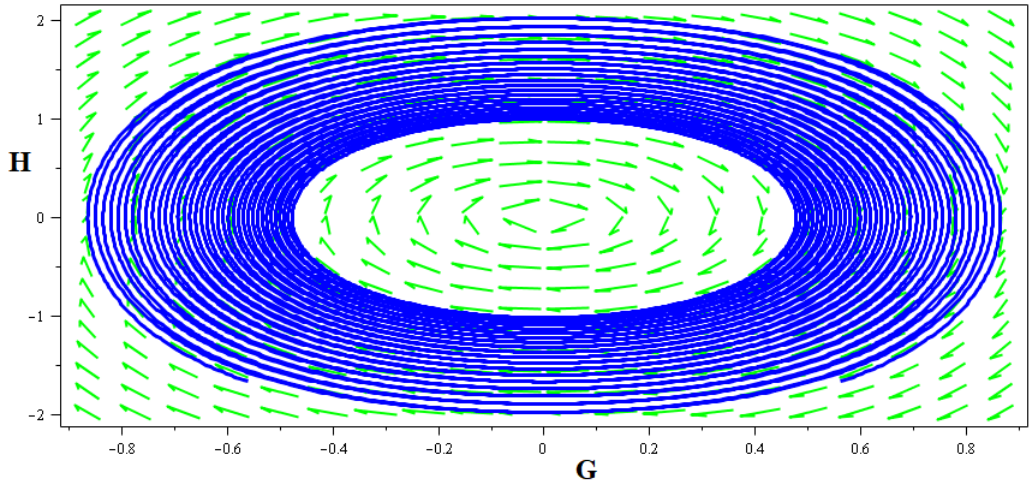

Figure 12: The visualization of phase portrait for (51) at $\mu_1 = 5, \mu_2 = 2, \mu_3 = 3, \chi = -5, \varsigma_1 = 5, \varsigma_2 = 1$.

Here in (56), k_0 and γ are the amplitude and the frequency the applied external force, respectively. We show the presence of periodic/chaotic behavior in the perturbed system in (56) for $(G(0) = 0, H(0) = 1)$ as initial condition and assigning arbitrary values to the involved free parameter in Figures 11 and 12.

Remarks In the case of $\Theta_1/\Theta_2 < 0$, the time-series plot in Figure. 13 shows quasi-periodic and fractal-like oscillations. The curve's this periodicity may be related to such structures as fractal-like periodic solitons will oscillate in both space and time. Analogously, the fractal-like periodic solitons are proved by the periodic oscillations with fractal structures at $\Theta_1/\Theta_2 > 0$ in Figure 14. Regular oscillations in chaotic systems prove that the system does not disappear into total chaos, but that despite their complexity and nonlinearity, produce predictable and regularly repeated patterns. Overall, all the time-series plots reveals that the system in (56) is fractal-like periodic.

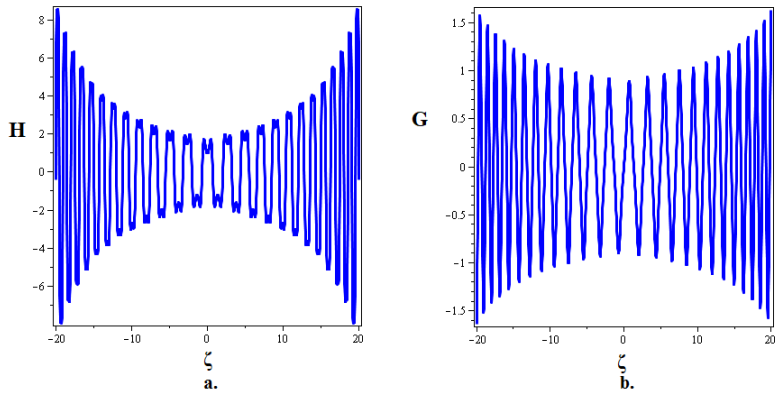

Figure 13: The time series plots of (56) for $\mu_1 = 0.10, \mu_2 = 0.20, \mu_3 = 0.20, \chi = 0.10, \varsigma_1 = 0.30, \varsigma_2 = 0.30, k_0 = 0.2, \gamma = 2\pi$.

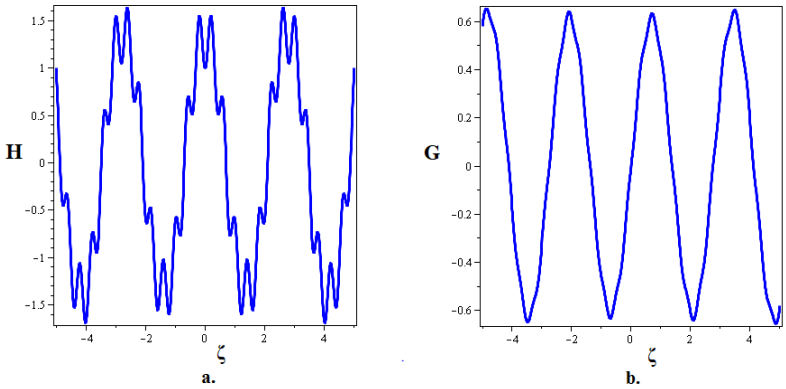

Figure 14: The time series plots of (56) for $\mu_1 = 5, \mu_2 = 2, \mu_3 = 3, \chi = -5, \varsigma_1 = 5, \varsigma_2 = 1, k_0 = 5, \gamma = 5\pi$.

6. Conclusion

In this work we have constructed some exact optical quasi-periodic soliton solutions for coupled NHEs via the effective unified method. We established rational, exponential, trigonometric and hyperbolic solutions. To show and explain the dynamical evolutions of the constructed optical solitons, we provided several 3D, 2D, and contour graphs under choices of the involved free parameters. These figures showed that the periodic and axial perturbations in the obtained quasi-periodic type solitons degenerate optical fractals. We also studied the Hamiltonian nature that gave positive fallout for quasi-periodicity and fractals for the governing system. The proposed optical solitons are expected to have many useful applications in the communication field. It is also worth noting that our used unified technique demonstrates its worth via presenting significant information of the coupled NHE dynamics, enlarging the family of optical soliton structures, and also unveiling potential applications in the field of nonlinear model management. It is important to

remember that the unified approach, however enlightening, has some limitations, even if it provided a significantly improved understanding of the soliton dynamics and of its relation to the models. Especially, the method fails if the highest order of the derivative and the nonlinear part are not uniformly balanced. Nevertheless, from the results, it can be concluded that the applied unified method is the one capable for various nonlinear model and it also relaxing as well as convenient for this kind of model. A future objective of the current work is to investigate soliton solutions for the proposed model in a stochastic and fractional context.

Funding

The authors extend their appreciation to the Arab Open University for funding this work through AOU research fund no. (AOUKSA-524008).

Acknowledgements

The author Khaled Suwais is grateful to the Arab Open University for facilitating this research work. The author N. Mlaiki would like to acknowledge Prince Sultan University for providing support through the TAS research lab.

References

[1] Leung, A. W. (2013). Systems of nonlinear partial differential equations: applications to biology and engineering (Vol. 49). Springer Science & Business Media.

[2] Rabinowitz, P. H. (1978). Some minimax theorems and applications to nonlinear partial differential equations. Nonlinear analysis, 161-177.

[3] Nofal, T. A. (2016). Simple equation method for nonlinear partial differential equations and its applications. Journal of the Egyptian Mathematical Society, 24(2), 204-209.

[4] Ji, X., Geng, H., Akhtar, N., & Yang, X. (2025). Floquet engineering of point-gapped topological superconductors. Physical Review B, 111, 195419.

[5] Guo, Y., Cao, X., Liu, B., & Gao, M. (2020). Solving partial differential equations using deep learning and physical constraints. Applied Sciences, 10(17), 5917.

[6] Mirhosseini-Alizamini, S. M., Rezazadeh, H., Eslami, M., Mirzazadeh, M., & Korkmaz, A. (2020). New extended direct algebraic method for the Tzitzica type evolution equations arising in nonlinear optics. Computational Methods for Differential Equations, 8(1), 28-53.

[7] Gozukizil, O. F., & Akcagil, S. (2013). The tanh-coth method for some nonlinear pseudoparabolic equations with exact solutions. Advances in Difference Equations, 2013(1), 143.

[8] Tsien, H. S. (1956). The Poincare-lighthill-kuo method. Advances in applied mechanics, 4, 281-349.

[9] Behera, S. (2024). Multiple soliton solutions of some conformable fractional nonlinear models using Sine-Cosine method. Optical and Quantum Electronics, 56(7), 1235.

[10] Liu, S., Fu, Z., Liu, S., & Zhao, Q. (2001). Jacobi elliptic function expansion method and periodic wave solutions of nonlinear wave equations. Physics Letters A, 289(1-2), 69-74.

[11] Tala-Tebue, E., Tsobgni-Fozap, D. C., Kenfack-Jiotsa, A., & Kofane, T. C. (2014). Envelope periodic solutions for a discrete network with the Jacobi elliptic functions and the alternative (G'/G)-expansion method including the generalized Riccati equation. The European Physical Journal Plus, 129(6), 136.

[12] Zayed, E. M. E., & Al-Nowehy, A. G. (2017). The Riccati equation method combined with the generalized extended (G'/G)-expansion method for solving the nonlinear KPP equation. J. Math. Res. Appl, 37, 577-590.

[13] Ali, R., and Tag-eldin, E. (2023). A comparative analysis of generalized and extended (G'/G)-Expansion methods for travelling wave solutions of fractional Maccari's system with complex structure. Alexandria Engineering Journal, 79, 508-530.

[14] Bibi, S., Mohyud-Din, S. T., Khan, U., & Ahmed, N. (2017). Khater method for nonlinear Sharma Tasso-Olever (STO) equation of fractional order. Results in physics, 7, 4440-4450.

[15] Wang, S. (2023). Novel soliton solutions of CNLSEs with Hirota bilinear method. Journal of Optics, 52(3), 1602-1607.

[16] Bekir, A., Aksoy, E., & Cevikel, A. C. (2015). Exact solutions of nonlinear time fractional partial differential equations by sub-equation method. Mathematical Methods in the Applied Sciences, 38(13), 2779-2784.

[17] Malik, S., Hashemi, M. S., Kumar, S., Rezazadeh, H., Mahmoud, W., & Osman, M. S. (2023). Application of new Kudryashov method to various nonlinear partial differential equations. Optical and Quantum Electronics, 55(1), 8.

[18] Jawad, A. J. A. M., Petkovic, M. D., & Biswas, A. (2010). Modified simple equation method for nonlinear evolution equations. Applied Mathematics and Computation, 217(2), 869-877.

[19] Lu, B. (2012). The first integral method for some time fractional differential equations. Journal of Mathematical Analysis and Applications, 395(2), 684-693.

[20] Raza, N., Rafiq, M. H., Kaplan, M., Kumar, S., & Chu, Y. M. (2021). The unified method for abundant soliton solutions of local time fractional nonlinear evolution equations. Results in Physics, 22, 103979.

[21] Kumar, A., & Kumar, S. (2023). Dynamic nature of analytical soliton solutions of the (1+ 1)-dimensional Mikhailov-Novikov-Wang equation using the unified approach. Int. J. Math. Comput. Eng, 1(2), 217-228.

[22] Abdeljawad, T. (2017). A Lyapunov type inequality for fractional operators with nonsingular Mittag-Leffler kernel. Journal of inequalities and applications, 2017(1), 130.

[23] Zhou, Y., Wang, J., Cao, L., Wang, G., Shi, Z., Lü, D., Huang, H., & Hu, C. (2024). Realization of chiral two-mode Lipkin–Meshkov–Glick models via acoustics. Reports on Progress in Physics, 87, 100502.

[24] Abdeljawad, T., & Baleanu, D. (2016). Discrete fractional differences with nonsingular discrete Mittag-Leffler kernels. Advances in Difference Equations, 2016(1), 232.

[25] Jarad, F., Abdeljawad, T., & Hammouch, Z. (2018). On a class of ordinary differential equations in the frame of Atangana–Baleanu fractional derivative. Chaos, Solitons & Fractals, 117, 16-20.

[26] Abraham, N. B., and Firth, W. J. (1990). Overview of transverse effects in nonlinear-optical systems. JOSA B, 7(6), 951-962.

[27] Alsaud, H., Youssoufa, M., Inc, M., Inan, I. E., and Bicer, H. (2024). Some optical solitons and modulation instability analysis of (3+1)-dimensional nonlinear Schrodinger and coupled nonlinear Helmholtz equations. Optical and Quantum Electronics, 56(7), 1138.

[28] Tamilselvan, K., Kanna, T., and Khare, A. (2016). Nonparaxial elliptic waves and solitary waves in coupled nonlinear Helmholtz equations. Communications in Nonlinear Science and Numerical Simulation, 39, 134-148.

[29] Singh, S., Kaur, L., Sakthivel, R., and Murugesan, K. (2020). Computing solitary wave solutions of coupled nonlinear Hirota and Helmholtz equations. Physica A: Statistical Mechanics and its Applications, 560, 125114.

[30] Saha, N., Roy, B., and Khare, A. (2021). Coupled Helmholtz equations: Chirped solitary waves. Chaos: An Interdisciplinary Journal of Nonlinear Science, 31(11).

[31] Borhan, J. R. M., Mamun Miah, M., Duraihem, F. Z., Iqbal, M. A., & Ma, W. X. (2024). New optical soliton structures, bifurcation properties, chaotic phenomena, and sensitivity analysis of two nonlinear partial differential equations. International Journal of Theoretical Physics, 63(8), 183.

[32] Hosseini, K., Hinçal, E., & Ilie, M. (2023). Bifurcation analysis, chaotic behaviors, sensitivity analysis, and soliton solutions of a generalized Schrödinger equation. Nonlinear Dynamics, 111(18), 17455-17462.

[33] Qi, J., Cui, Q., Zhang, L., & Sun, Y. (2023). Solution structures of an electrical transmission line model with bifurcation and chaos in hamiltonian dynamics. International Journal of Bifurcation and Chaos, 33(09), 2350108.

[34] Hossain, M. N., Miah, M. M., Duraihem, F. Z., Rehman, S., & Ma, W. X. (2024). Chaotic behavior, bifurcations, sensitivity analysis, and novel optical soliton solutions to the Hamiltonian amplitude equation in optical physics. Physica Scripta, 99(7), 075231.

[35] Wang, K. (2021). A new fractal model for the soliton motion in a microgravity space. International Journal of Numerical Methods for Heat & Fluid Flow, 31(1), 442-451.

[36] Martin-Vergara, F., Rus, F., & Villatoro, F. R. (2021). Fractal structure of the soliton scattering for the graphene superlattice equation. Chaos, Solitons & Fractals, 151, 111281.

[37] Zheng, C. L. (2003). Coherent soliton structures with chaotic and fractal behaviors in a generalized (2+ 1)-dimensional Korteweg de-Vries system. Chinese Journal of Physics, 41(5), 442-455.

[38] Stanley, H. E. (1992). Fractal landscapes in physics and biology. Physica A: Statistical Mechanics and its Applications, 186(1-2), 1-32.

[39] Bunde, A., & Havlin, S. (Eds.). (2013). Fractals in science. Springer.
[40] Bizzarri, M., Giuliani, A., Cucina, A., DAnselmi, F., Soto, A. M., & Sonnenschein, C. (2011, June). Fractal analysis in a systems biology approach to cancer. In Seminars in cancer biology (Vol. 21, No. 3, pp. 175-182). Academic Press.